Inorganic Chemistry

pubs.acs.org/IC

Article

Switch of Thermal Expansions Triggered by Itinerant Electrons in Isostructural Metal Trifluorides

Feiyu Qin, Xiaoying Wang, Lei Hu,* Ning Jia, Zhibin Gao,* Umut Aydemir, Jun Chen,* Xiangdong Ding, and Jun Sun

Cite This: *Inorg. Chem.* 2022, 61, 21004−21010

Read Online

ACCESS | Metrics & More | Article Recommendations | Supporting Information

ABSTRACT: Manageable thermal expansion (MTE) of metal trifluorides can be achieved by introducing local structure distortion (LSD) in the negative thermal expansion ScF_3. However, an open issue is why isostructural TiF_3, free of LSD, exhibits positive thermal expansion. Herein, a combined analysis of synchrotron X-ray diffraction, X-ray pair distribution function, and rigorous first-principles calculations was performed to reveal the important role of itinerant electrons in mediating soft phonons and lattice dynamics. Metallic TiF_3 demonstrates itinerant electrons and a suppressed Grüneisen parameter $\gamma \approx -20$, while insulating ScF_3 absence of itinerant electrons has a considerable $\gamma \approx -120$. With increasing electron doping concentrations in ScF_3, soft phonons become hardened and the γ is repressed significantly, identical to TiF_3. The presented results update the thermal expansion transition mechanism in framework structure analogues and provide a practical approach to obtaining MTE without inducing sizable structure distortion.

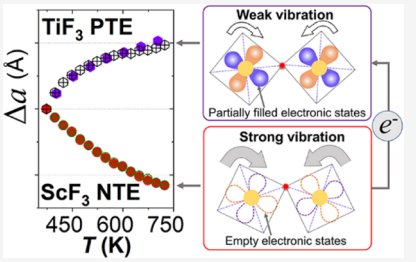

1. INTRODUCTION

Negative thermal expansion (NTE) is an uncommon physical phenomenon, denoting that the crystal lattice volume contracts upon heating.[1,2] By diverse chemical modifications, manageable thermal expansion (MTE) could be attained based on NTE, including compelling zero thermal expansion (ZTE).[3−9] MTE is vital for electronic and optical devices with superior size accuracy, such as laser gyroscopes, mirrors of lithography machines, space telescopes, and so forth. A full understanding of the fundamental factors of modifying the NTE is the prerequisite for achieving MTE.

Materials with NTE are rare and could be categorized by diverse mechanisms, such as magnetic order in a FeNi Invar alloy,[4] rare-earth intermetallic alloys,[10−12] MnM′Ge-based alloys (M′ = Co or Ni),[13,14] anti-perovskite nitrides,[15] spontaneous polarization in $PbTiO_3$-based ferroelectric solids,[16−18] strong covalent binding in VB_2,[44] chemical pressure,[45] charge or orbital ordering in (Bi, La)NiO_3,[19] Ca_2RuO_4,[20] and V_2OPO_4,[21] and so forth. Among them, NTE derived from soft optical phonons with negative Grüneisen parameters (γ) is a dominating branch, such as the prototype ZrW_2O_8,[22] open-framework oxides,[23,24] cyanides,[25,26] metal−organic frameworks,[27] and equally attractive cubic fluorides.[28−30] Owing to the critical role of soft optical phonons, to achieve MTE of open-framework solids, long-term cognition focuses on developing diverse chemical methods to mediate the specific phonon modes by introducing local structure distortion (LSD) in NTE materials. These methods include chemical substitution,[31] nano-scale engineerings,[32] electrochemical intercalations,[33] and so forth. The critical factor is to construct LSD,[34] which demonstrates distinct phonon anharmonicity (quantified by γ) and thermal expansions, deviating from the average crystal structure. The deliberately designed LSD is capable of transforming NTE into ZTE and PTE, thus realizing MTE, which gradually becomes the exclusive nature to explain MTE in open framework derivatives and homologous series.

It is well known that cubic ScF_3 reveals a prominent NTE. However, an open issue is why the isostructural TiF_3, free of LSD, exhibits a completely disparate positive thermal expansion (PTE). One may wonder how the NTE in ScF_3 could switch to PTE in TiF_3 without introducing any LSD between them. Cubic ScF_3 and TiF_3 share considerable similarities in cationic sizes, masses, electronegativities, disorder magnetism (diamagnetism and paramagnetism, respectively), and the absence of LSD. Strikingly, the different electronic configurations of Sc^{3+} ($3d^0$) and Ti^{3+} ($3d^1$) for insulating ScF_3 and metallic TiF_3 lead to the absence and presence of itinerant electrons, respectively. One may expect that the existence of itinerant electrons could mediate soft phonons and thus be a fundamental aspect driving such disparate thermal expansions in cubic ScF_3 and TiF_3. However, there is neither experimental observation nor theoretical prediction concerning the impact of itinerant electrons on

Received: October 3, 2022
Published: December 15, 2022

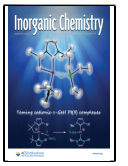

soft phonons for tuning thermal expansions in framework structure solids.

Herein, we have performed a joint study of experimental and theoretical lattice dynamics on isostructural trifluorides, the cubic ScF_3 and TiF_3, to unveil the interaction between itinerant electrons and soft phonons, a phenomenon that has never been reported in framework structure fluorides. Synchrotron X-ray techniques confirm the NTE and flexible Sc···F atomic pairs in cubic ScF_3, in sharp contrast to the PTE and stiff Ti···F atomic pair in cubic TiF_3, respectively. Electronic band structure investigation shows the partially occupied antibonding states in metallic TiF_3, confirming the existence of itinerant electrons. Meanwhile, ScF_3 is a wide band gap insulator with empty antibonding states. Phonon dispersion shows soft optical phonons become hardened, and their negative γ are substantially suppressed in TiF_3 compared to a remarkably large magnitude of negative γ in ScF_3. Furthermore, the identical changes in soft phonons (phonon hardening and negative γ suppressing) are also reemergent by doping electrons in the host matrix of ScF_3. This work reports the impact of itinerant electrons on soft phonons in framework structure fluorides. This unusual impact could be utilized to adjust NTE to achieve remarkable MTE in high-end electronic devices, which could retain high charge mobilities by avoiding the scattering induced by structure distortions.

2. RESULTS AND DISCUSSION

ScF_3 demonstrates a cubic structure (space group, $Pm\bar{3}m$) over a broad temperature range (Figure S1a). According to synchrotron X-ray diffraction (SXRD) results, TiF_3 also reveals the same cubic structure above 373 K, below which it undergoes a phase transition into rhombohedral symmetry (Supporting Information, Figure S1b,c), also in line with the previous study.[35,42] Regarding the cubic structure, Sc or Ti occupies the Wyckoff site 1*a* (0,0,0), and F locates at the site of 1*b* (0.5, 0, 0). Sc or Ti octahedrally coordinates to six equivalent fluorine atoms to form a corner-sharing framework structure, as illustrated by the inset of Figure 1a.

Figure 1a shows the disparate thermal expansions observed in the two isostructural metal trifluorides, which are extracted from the structure refinement on SXRD and X-ray pair distribution function (XPDF) data shown in Figures S2 and S3. As the temperature gradually increases from 373 to 723 K, the relative lattice constant Δa of ScF_3 (in the red filled and olive crossed circles) decreases gradually with increasing temperature, confirming the strong NTE with the coefficient of thermal expansion (CTE) of -3.30×10^{-6}/K (obtained from XPDF data). In sharp contrast, the Δa of cubic TiF_3 (in purple filled and black crossed hexagons) exhibits a smooth increase, with a positive CTE of $+2.87 \times 10^{-6}$/K from 373 to 723 K (obtained from XPDF data). Atomic displacement parameters of fluorine atoms parallel (F_U_{11}) and perpendicular (F_U_{33}) to the M−F (M = Sc or Ti) bonds are extracted and compared in Figure 1b. The F_U_{33} of ScF_3 (olive crossed circle) increases considerably with increasing temperature, suggesting a strong thermal vibration perpendicular to the Sc−F bond. In contrast, both the F_U_{11} and F_U_{33} (half-filled blue hexagon and circle) of TiF_3 are insensitive to temperature. These results demonstrate a strong transverse thermal vibration of fluorine atoms in ScF_3 in line with previous work,[36] whereas only a weak transverse thermal vibration is observed in TiF_3. This can be schematically illustrated by the large anisotropic and near-isotropic thermal ellipsoids of fluorine atoms in Figure 1c.

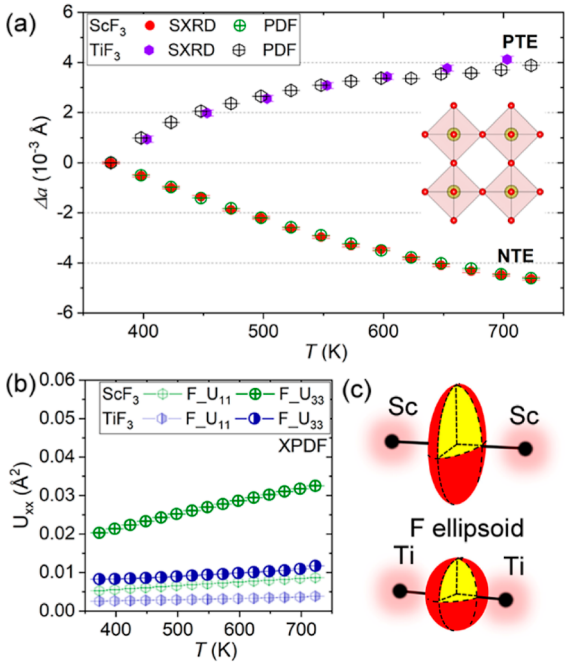

Figure 1. Temperature dependence of (a) relative lattice constant Δa in ScF_3 and TiF_3. (b) Atomic displace parameters of fluorine atoms, parallel (F_U_{11}) and perpendicular (F_U_{33}) to M−F bond (M = Sc or Ti). (c) Schematic illustration of fluorine thermal ellipsoids.

To understand the contrasting thermal expansions from a perspective of local vibration dynamics, XPDF analysis was performed. Figure 2a,b shows the temperature dependence of the radial distribution function, $R(r)$, for different r ranges. The

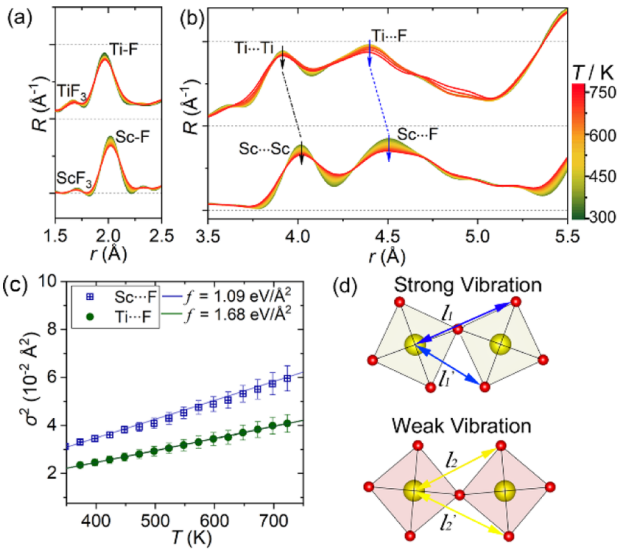

Figure 2. (a,b) Temperature dependence of the XPDF radial distribution function $R(r)$, in which M−F, M−M, and M···F atomic pairs are indicated (M = Sc and Ti atoms in yellow color, F atoms in red color). (c) Square of peak width $\sigma^2(T)$ and force constant f of Sc···F and Ti···F atomic pairs. (d) Strong and weak vibration models for ScF_6 and TiF_6 octahedra, respectively. The distances of M···F atomic pairs are marked by two-ended arrows and denoted by l_i and l_i' (i = 1 and 2).

https://doi.org/10.1021/acs.inorgchem.2c03499
Inorg. Chem. 2022, 61, 21004−21010

nearest-neighboring (NN) Ti−F and Sc−F peaks are located at 1.96 and 2.02 Å as shown in Figure 2a. The second NN Ti···Ti and Sc−Sc peaks are at 3.91 and 4.02 Å, marked by black arrows in Figure 2b. Close to 4.40 and 4.51 Å are the third NN Ti···F and Sc···F peaks. TiF_3 has a smaller total bond distance of M−F pairs than ScF_3 (M = Ti or Sc). It should be noted that both the Sc−F and Ti−F peaks, in the low r range from 1.70 to 2.25 Å, maintain a symmetric peak profile without additional shoulders emerging with the temperature rising. This confirms the absence of LSD in TiF_3, although TiF_3 undergoes a phase transition from a rhombohedral to a cubic structure around 370 K. Compared to Sc−Sc and Sc···F in ScF_3, the atomic pairs Ti···Ti and Ti···F in TiF_3 shift to a low r region (shown by the dashed lines) from 3.65 to 5.25 Å, in good agreement with the smaller unit cell in TiF_3. More significantly, the Sc−Sc and Sc···F peaks in ScF_3 decrease in peak intensity and broaden in width as temperature increases. Meanwhile, the change of peak intensity and width for Ti···Ti and Ti···F peaks in TiF_3 is minor.

In Figure 2c, the square of Gaussian peak width σ^2 for Ti···F and Sc···F peaks is presented. The σ^2 of Sc···F (blue crossed box) improves significantly than that of Ti···F (olive filled circle) as the temperature rises. The force constant f of M···F atomic pairs could be quantitatively determined by utilizing the correlated Einstein model, indicated by the blue and olive lines. The fitting details are presented in Section 6 of the Supporting Information. The corresponding f of Ti···F and Sc···F are 1.68 and 1.09 eV/Å^2, corroborating a stiffer Ti···F and a flexible Sc···F atomic pair. The weak correlation of Sc···F atomic pairs allows a stronger dynamic vibration of corner-shared octahedra ScF_6 in ScF_3 (Figure 2d), which agrees well with the large F_U_{33} observed in Figure 1b. This strong vibration gives rise to temperature-sensitive distance distributions of the Sc···F atomic pair denoted by a large difference in transient atomic distances, l_1 and l_1' (blue arrows). For the case in TiF_3, the dynamical vibration seems to be impeded and only temperature-insensitive distance distributions of Ti···F atomic pair could be observed with nearly similar atomic distances l_2 and l_2' (yellow arrows) shown in Figure 2d. These strong and weak vibration models of ScF_3 and TiF_3 are also in line with their different total band distances of M−F pairs. Besides, in this vibration model, the F−F bonding may also be important in affecting the dynamic vibration of octahedra. A detailed understanding of the F−F bonding is reported by a thorough examination based on a neutron scattering study.[47] Nevertheless, the main difference in vibrational dynamics between ScF_3 and TiF_3 is confirmed by the characteristics of the M−M and M−F atomic pairs.

These local vibration dynamics provide an intuitive understanding of essentially different thermal expansions in ScF_3 and TiF_3. However, the nature leading to the strong discrepancy in local vibration dynamics is still to be resolved. Sc^{3+} and Ti^{3+} in ScF_3 and TiF_3, located at the NN positions in the periodic table, share similar cation sizes, atomic masses, and electronegativities. ScF_3 and TiF_3 demonstrate the same cubic structure at high temperatures. Moreover, since the ScF_3 and TiF_3 demonstrate diamagnetism and paramagnetism at least above 200 K (MT curve in Figure S5, Supporting Information), it is unlikely that the different thermal expansion here is affected by these magnetic disorder states.[8,43] The obvious distinction between ScF_3 and TiF_3 is the electronic configuration, that is, the absence and presence of itinerant electrons (will be discussed below). Given that outer-shell electrons determine the properties of most materials, it is reasonable to assume that this difference in itinerant electrons between ScF_3 and TiF_3 plays a critical role, resulting in disparate lattice thermal expansions. We first examine the difference in chemical binding and chemical pressure of these two compounds. From the electron density map shown in Figure S8, it can be confirmed that there is less covalent binding between either Sc/Ti−F or F−F, which coincides with the previous consensus that bonding in ScF_3 is more ionic. Thus, the strong covalent binding in VB_2 controlling the thermal expansion is not significant in our case. Besides, the chemical pressure of TiF_3 is calculated to be −0.104 GPa and that of ScF_3 is 0.101 GPa, demonstrating the similar magnitude of chemical pressures of the two metal trifluorides (Supporting Information).

To investigate the differences in the electronic band structures and phonon structures of cubic ScF_3 and TiF_3, we employed the first-principles method. A large band gap is observed in ScF_3 as shown in Figure 3a,b, confirming its

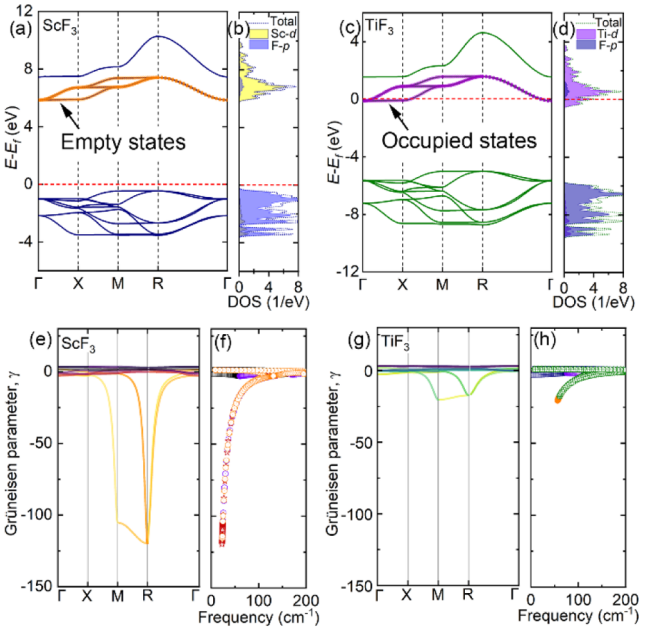

Figure 3. (a) Band structure and (b) density of states (DOSs) for cubic ScF_3. (c) Band structure and (d) DOS for cubic TiF_3. The lower-energy CBs in cubic ScF_3 and TiF_3 are highlighted in orange and purple dotted lines, respectively. The Fermi level, E_f, is denoted by the red dotted line. (e) Grüneisen parameter (γ) for phonon modes along with high symmetry directions and (f) γ as a function of the phonon frequency for ScF_3. (g) γ for the phonon modes and (h) γ as a function of frequency for TiF_3.

insulating feature. The conduction band (CB) is composed of the hybridized Sc d orbitals and F p orbitals. The Fermi level, E_f (red dotted line), is far away from the lower-energy CB (shown by the orange dotted line), indicating the feature of empty antibonding states marked by the black arrow. In sharp contrast, the E_f touches the CB minimum of TiF_3 highlighted by the purple dotted line, confirming its metallic feature and the existence of itinerant electrons. As shown in Figure S5, ScF_3 and TiF_3 demonstrate extremely low and high absorbance for visible and infrared light, consistent with their features of different electronic structures. In addition, the antibonding

https://doi.org/10.1021/acs.inorgchem.2c03499
Inorg. Chem. 2022, 61, 21004−21010

states are partially occupied, which tends to affect the band order and thus the bond forces of atomic pairs.

It is well known that γ is the measurement of phonon anharmonicity.[37] Phonon modes with negative γ contribute to the lattice NTE. Here, γ dispersions of ScF_3 and TiF_3 have been calculated and are compared in Figure 3e–h. As regards ScF_3, soft phonon modes at high-symmetry points, M and R, demonstrate a sizable magnitude of negative γ values, such as −105.4 and −119.6 in Figure 3e. It should be noted that these specific phonons correspond to ScF_6 octahedron rotations and are responsible for the strong NTE in ScF_3.[38,39] Figure 3f shows that the phonons with a considerably large magnitude of negative γ are dominated by low-frequency phonons, especially lower than 50 cm^{-1}. By contrast, the magnitude of the γ values of the phonon modes at M and R points in TiF_3 decreases substantially, merely limited to −20.4 and −17.3, respectively. Furthermore, these soft phonons with negative γ values are absent in frequencies lower than 50 cm^{-1} as shown in Figure 3h.

The notable reduction in the magnitude of the negative γ values and the complete absence of specific soft phonons below 50 cm^{-1} in TiF_3 demonstrate the considerably suppressed NTE contribution. This suppressed NTE contribution is easily overwhelmed by the PTE contribution from high-frequency optical phonons, which ultimately leads to the global lattice PTE of TiF_3. These theoretical results are in good agreement with the experimental data of local vibration dynamics shown in Figure 2. In short, compared to the wide band gap feature of insulating ScF_3, the existence of itinerant electrons in metallic TiF_3 with partially occupied antibonding states has a close relationship with the suppressed phonon anharmonicity.

To further confirm the phonon differences exclusively originated from itinerant electrons, we directly added electrons into the host matrix of ScF_3 with doping concentrations (n_c) of 0.25 and 0.50 e/f.u. (e, electron; f.u., formula unit). Figure S6a shows the robust phonon dispersion of ScF_3 at a 0.25 e/f.u. concentration without imaginary frequencies, confirming the structure stability after electron doping. Soft phonon modes located at M and R points are highlighted by the orange circle and olive hexagon. For clarity, the high-frequency phonons are marked by red circles, assigned to longitudinal vibrations of the Sc–F atomic pairs, and contribute to PTE. The phonon dispersion of ScF_3 is shown in Figure 4a. Figure 4b shows that γ values of specific phonon modes at M and R points diminish notably with the enhancement of n_c from 0.25 e/f.u. (left panel) to 0.50 e/f.u. concentrations (right panel). Figure 4c shows the frequency dependence of the γ values of electron-doped ScF_3. Soft phonons with negative γ in ScF_3 at a 0.5 e/f.u concentration (olive hexagon) are absent in a frequency lower than 75 cm^{-1} compared to its counterpart at a 0.25 e/f.u. concentration (orange circle). Figure 4d shows the frequency changes of specific soft phonon modes at M and R points in pristine and electron-doped ScF_3. These soft phonons become hardened with electron doping. Meanwhile, the γ values of these soft phonon modes are substantially repressed with doping more electrons. As shown in Figure 4e, the γ values at M and R points are repressed substantially from −105.4 and −119.6 in pristine ScF_3 to −19.1 and −15.8 in doped ScF_3 at a 0.25 e/f.u. concentration, and continuously decline to around −7.2 and −6.5 at a 0.50 e/f.u concentration.

Therefore, the gradual electron doping in ScF_3 can enhance the electron–phonon coupling and thus drive the hardening of

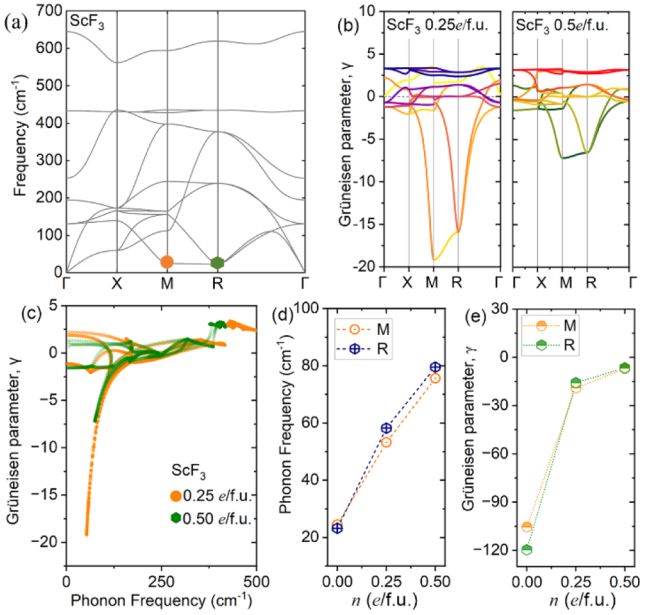

Figure 4. (a) Phonon dispersion of electron-doped ScF_3 at a 0.25 e/f.u. concentration. The lowest phonon modes located at high-symmetry points, M and R, are marked by the orange circle and olive hexagon. Low- and high-frequency phonons are highlighted in olive and red. (b) γ phonon dispersion of ScF_3 at 0.25 and 0.5 e/f.u. concentrations. (c) γ as a function of phonon frequency of ScF_3 at 0.25 and 0.5 e/f.u. concentrations. (d) Phonon frequency of modes at M and R points as a function of the electron doping concentration (n_c) in doped ScF_3. (e) γ of modes at M and R points as a function of n_c in doped ScF_3.

specific soft phonons and the concomitant suppression of phonon anharmonicity, reproducing the results found in TiF_3. The itinerant electrons in TiF_3 could somehow affect the thermal vibration of fluorine atoms, resulting in a stiffer Ti···F atomic pair compared to a flexible Sc···F atomic pair in ScF_3. One possible reason is that the Coulomb repulsion between itinerant electrons and fluorine anions "blocks" the vibrations of fluorine atoms. This results in a larger force constant f of M···F pairs in TiF_3 than in ScF_3. These statements were supported by the experimental data of local vibration dynamics and calculation results of the effects of itinerant electrons on specific phonon modes. As a consequence, itinerant electrons could be utilized to modulate soft phonons and thus impose a sufficient impact on thermal expansion, even switching the NTE of ScF_3 into the PTE of TiF_3. Actually, the interaction between electrons and phonons could be quantized, which is strongly band-dependent and acts principally on partially filled 3d states with itinerant electrons compared to other completely filled or empty 3d states.[40,46]

Note that the LSD is a well-developed strategy and plays a critical role in tuning NTE in framework structure solids. Especially, it is suitable for considerable size differences between host and substitutional elements, such as substituting Sc with Ga, Fe, or Al in the host matrix of ScF_3.[34,41] As regards cutting-edge electronic devices, they require MTE as well as superior charge mobilities. This requires avoiding charge scattering to the greatest extent. Actually, the designed LSD inevitably introduces short-range structure defects, resulting in charge scattering and thus is disadvantageous to mobilities. Unlike LSD, the introduction of itinerant electrons does not result in a considerable structure distortion, which is especially

https://doi.org/10.1021/acs.inorgchem.2c03499
Inorg. Chem. 2022, 61, 21004−21010

critical for the synergistic achievement of MTE and high mobilities.

3. CONCLUSIONS

In summary, the combined experimental and theoretical analyses ascertain the impact of itinerant electrons on a soft phonon in representative framework structures, electron-doped ScF_3 and TiF_3. ScF_3 reveals prominent NTE with a considerably large anisotropic fluorine thermal ellipsoid, strong ScF_6 octahedron vibration, and soft Sc···F atomic pairs, corresponding to the large phonon anharmonicity confirmed by the phonon structure calculation. In contrast, the isostructural TiF_3 demonstrates disparate PTE with the isotropic-like fluorine thermal ellipsoid, weakened TiF_6 octahedron vibration, and stiff Ti···F atomic pairs, corresponding to the soft phonon hardening and the suppressed magnitude of negative γ.

Intriguingly, phonon hardening and the suppression in the magnitude of negative γ observed in TiF_3 are equally identified in electron-doped ScF_3. With the gradual increase in the electron doping concentrations, soft phonons become more hardened, and the magnitude of the negative γ continues to be suppressed. These results elucidate the vital impact of itinerant electrons on soft phonons, updating the mechanism of thermal expansion switch in framework structure fluorides. This impact is sufficient to affect the NTE by modulating the electron concentration, which provides an unconventional perspective on achieving MTE by mediating itinerant electrons.

■ ASSOCIATED CONTENT

Supporting Information

The Supporting Information is available free of charge at https://pubs.acs.org/doi/10.1021/acs.inorgchem.2c03499.

Experimental details, DFT calculation, synchrotron XRD, XPDF, magnetic measurement, UV−vis absorbance spectrum, the correlated Einstein model, the calculated phonon dispersions and electron density map, and the chemical pressure (PDF)

■ AUTHOR INFORMATION

Corresponding Authors

Lei Hu − *State Key Laboratory for Mechanical Behavior of Materials, Xi'an Jiaotong University, Xi'an 710049, China;* orcid.org/0000-0002-4647-1604; Email: leihu@xjtu.edu.cn

Zhibin Gao − *State Key Laboratory for Mechanical Behavior of Materials, Xi'an Jiaotong University, Xi'an 710049, China;* orcid.org/0000-0002-6843-381X; Email: zhibin.gao@xjtu.edu.cn

Jun Chen − *Department of Physical Chemistry, University of Science and Technology Beijing, Beijing 100083, China;* orcid.org/0000-0002-7330-8976; Email: junchen@ustb.edu.cn

Authors

Feiyu Qin − *State Key Laboratory for Mechanical Behavior of Materials, Xi'an Jiaotong University, Xi'an 710049, China*

Xiaoying Wang − *State Key Laboratory for Mechanical Behavior of Materials, Xi'an Jiaotong University, Xi'an 710049, China*

Ning Jia − *School of Materials Science and Engineering, Nanyang Technological University, Singapore 639798, Singapore*

Umut Aydemir − *Department of Chemistry, Koç University, Istanbul 34450, Turkey; Koç University Boron and Advanced Materials Application and Research Center (KUBAM), Istanbul 34450, Turkey;* orcid.org/0000-0003-1164-1973

Xiangdong Ding − *State Key Laboratory for Mechanical Behavior of Materials, Xi'an Jiaotong University, Xi'an 710049, China*

Jun Sun − *State Key Laboratory for Mechanical Behavior of Materials, Xi'an Jiaotong University, Xi'an 710049, China*

Complete contact information is available at: https://pubs.acs.org/10.1021/acs.inorgchem.2c03499

Author Contributions

All authors have approved the final version of the manuscript.

Notes

The authors declare no competing financial interest.

■ ACKNOWLEDGMENTS

We acknowledge the financial support of the National Natural Science Foundation of China (no. 22205171) and the Top Young Talents Program of Xi'an Jiaotong University. This work was also supported by KAKENHI grants (JP 19F19057) from the Japan Society for the Promotion of Science (JSPS). Z.G. acknowledges the support of the National Natural Science Foundation of China (no. 12104356), China Postdoctoral Science Foundation (no. 2022M712552), the Opening Project of Shanghai Key Laboratory of Special Artificial Microstructure Materials and Technology (Ammt2022B-1), and the Fundamental Research Funds for the Central Universities. We also acknowledge the support by HPC Platform, Xi'an Jiaotong University. We thank Dr. Yue-Wen Fang for the discussions and Dr. A. A. Yakovenko for the SXRD data collection.

■ REFERENCES

(1) Dolling, G.; Cowley, R. The thermodynamic and optical properties of germanium, silicon, diamond and gallium arsenide. *Proc. Phys. Soc.* **1966**, *88*, 463.

(2) Li, Q.; Lin, K.; Liu, Z.; Hu, L.; Cao, Y.; Chen, J.; Xing, X. Chemical Diversity for Tailoring Negative Thermal Expansion. *Chem. Rev.* **2022**, *122*, 8438−8486.

(3) Roy, R.; Agrawal, D. K.; McKinstry, H. A. Very low thermal expansion coefficient materials. *Annu. Rev. Mater. Sci.* **1989**, *19*, 59−81.

(4) Mohn, P. A century of zero expansion. *Nature* **1999**, *400*, 18−19.

(5) Sleight, A. Zero-expansion plan. *Nature* **2003**, *425*, 674−676.

(6) Chen, J.; Xing, X.; Sun, C.; Hu, P.; Yu, R.; Wang, X.; Li, L. Zero thermal expansion in $PbTiO_3$-based perovskites. *J. Am. Chem. Soc.* **2008**, *130*, 1144−1145.

(7) Song, X.; Sun, Z.; Huang, Q.; Rettenmayr, M.; Liu, X.; Seyring, M.; Li, G.; Rao, G.; Yin, F. Adjustable zero thermal expansion in antiperovskite manganese nitride. *Adv. Mater.* **2011**, *23*, 4690−4694.

(8) Hu, L.; Chen, J.; Fan, L.; Ren, Y.; Rong, Y.; Pan, Z.; Deng, J.; Yu, R.; Xing, X. Zero Thermal Expansion and Ferromagnetism in Cubic $Sc_{1-x}M_xF_3$ (M = Ga, Fe) over a Wide Temperature Range. *J. Am. Chem. Soc.* **2014**, *136*, 13566−13569.

(9) Hu, L.; Chen, J.; Xu, J.; Wang, N.; Han, F.; Ren, Y.; Pan, Z.; Rong, Y.; Huang, R.; Deng, J.; Li, L.; Xing, X. Atomic linkage flexibility tuned isotropic negative, zero, and positive thermal expansion in $MZrF_6$ (M = Ca, Mn, Fe, Co, Ni, and Zn). *J. Am. Chem. Soc.* **2016**, *138*, 14530−14533.

(10) Song, Y.; Chen, J.; Liu, X.; Wang, C.; Zhang, J.; Liu, H.; Zhu, H.; Hu, L.; Lin, K.; Zhang, S.; Xing, X. Zero thermal expansion in magnetic and metallic Tb (Co, Fe) $_2$ intermetallic compounds. *J. Am. Chem. Soc.* **2018**, *140*, 602−605.
(11) Cao, Y.; Lin, K.; Khmelevskyi, S.; Avdeev, M.; Taddei, K. M.; Zhang, Q.; Huang, Q.; Li, Q.; Kato, K.; Tang, C. C.; Gibbs, A.; Wang, C. W.; Deng, J.; Chen, J.; Zhang, H.; Xing, X. Ultrawide Temperature Range Super-Invar Behavior of R_2 (Fe, Co)$_{17}$ Materials (R= Rare Earth). *Phys. Rev. Lett.* **2021**, *127*, 055501.
(12) Song, Y.; Sun, Q.; Xu, M.; Zhang, J.; Hao, Y.; Qiao, Y.; Zhang, S.; Huang, Q.; Xing, X.; Chen, J. Negative thermal expansion in (Sc, Ti) Fe_2 induced by an unconventional magnetovolume effect. *Mater. Horiz.* **2020**, *7*, 275−281.
(13) Shen, F.; Zhou, H.; Hu, F.; Wang, J.-T.; Deng, S.; Wang, B.; Wu, H.; Huang, Q.; Wang, J.; Chen, J.; He, L.; Hao, J.; Yu, Z.; Liang, F.; Liang, T.; Sun, J.; Shen, B. Cone-spiral magnetic ordering dominated lattice distortion and giant negative thermal expansion in Fe-doped MnNiGe compounds. *Mater. Horiz.* **2020**, *7*, 804−810.
(14) Zhao, Y.-Y.; Hu, F.-X.; Bao, L.-F.; Wang, J.; Wu, H.; Huang, Q.-Z.; Wu, R.-R.; Liu, Y.; Shen, F.-R.; Kuang, H.; Zhang, M.; Zuo, W.-L.; Zheng, X.-Q.; Sun, J.-R.; Shen, B.-G. Giant negative thermal expansion in bonded MnCoGe-based compounds with Ni_2In-type hexagonal structure. *J. Am. Chem. Soc.* **2015**, *137*, 1746−1749.
(15) Takenaka, K.; Takagi, H. Giant negative thermal expansion in Ge-doped anti-perovskite manganese nitrides. *Appl. Phys. Lett.* **2005**, *87*, 261902.
(16) Chen, J.; Fan, L. L.; Ren, Y.; Pan, Z.; Deng, J. X.; Yu, R. B.; Xing, X. R. Unusual Transformation from Strong Negative to Positive Thermal Expansion in $PbTiO_3$-$BiFeO_3$ Perovskite. *Phys. Rev. Lett.* **2013**, *110*, 115901.
(17) Chen, J.; Nittala, K.; Forrester, J. S.; Jones, J. L.; Deng, J. X.; Yu, R. B.; Xing, X. R. The Role of Spontaneous Polarization in the Negative Thermal Expansion of Tetragonal $PbTiO_3$-Based Compounds. *J. Am. Chem. Soc.* **2011**, *133*, 11114−11117.
(18) Pan, Z.; Chen, J.; Yu, R. Z.; Patra, L.; Ravindran, P.; Sanson, A.; Milazzo, R.; Carnera, A.; Hu, L.; Wang, L.; Yamamoto, H.; Ren, Y.; Huang, Q. Z.; Sakai, Y.; Nishikubo, T.; Ogata, T.; Fan, X. A.; Li, Y. W.; Li, G. Q.; Hojo, H.; Azuma, M.; Xing, X. R. Large Negative Thermal Expansion Induced by Synergistic Effects of Ferroelectrostriction and Spin Crossover in $PbTiO_3$-Based Perovskites. *Chem. Mater.* **2019**, *31*, 1296−1303.
(19) Azuma, M.; Chen, W. T.; Seki, H.; Czapski, M.; Olga, S.; Oka, K.; Mizumaki, M.; Watanuki, T.; Ishimatsu, N.; Kawamura, N.; Ishiwata, S.; Tucker, M. G.; Shimakawa, Y.; Attfield, J. P. Colossal negative thermal expansion in $BiNiO_3$ induced by intermetallic charge transfer. *Nat. Commun.* **2011**, *2*, 347.
(20) Qi, T. F.; Korneta, O. B.; Parkin, S.; De Long, L. E.; Schlottmann, P.; Cao, G. Negative Volume Thermal Expansion Via Orbital and Magnetic Orders in $Ca_2Ru_{1-x}Cr_xO_4$($0 < x < 0.13$). *Phys. Rev. Lett.* **2010**, *105*, 177203.
(21) Pachoud, E.; Cumby, J.; Lithgow, C. T.; Attfield, J. P. Charge Order and Negative Thermal Expansion in V_2OPO_4. *J. Am. Chem. Soc.* **2018**, *140*, 636−641.
(22) Mary, T. A.; Evans, J. S. O.; Vogt, T.; Sleight, A. W. Negative thermal expansion from 0.3 to 1050 Kelvin in ZrW_2O_8. *Science* **1996**, *272*, 90−92.
(23) Shi, N.; Sanson, A.; Gao, Q.; Sun, Q.; Ren, Y.; Huang, Q.; de Souza, D. O.; Xing, X.; Chen, J. Strong negative thermal expansion in a low-cost and facile oxide of $Cu_2P_2O_7$. *J. Am. Chem. Soc.* **2020**, *142*, 3088−3093.
(24) Zhang, M. D.; Mao, Y. C.; Guo, J.; Zhou, W. J.; Chao, M. J.; Zhang, N.; Yang, M. J.; Kong, X. H.; Kong, X. S.; Liang, E. J. A novel negative thermal expansion material of $Zr_{0.70}V_{1.33}Mo_{0.67}O_{6.73}$. *RSC Adv.* **2017**, *7*, 3934−3940.
(25) Gao, Q.; Wang, J.; Sanson, A.; Sun, Q.; Liang, E.; Xing, X.; Chen, J. Discovering large isotropic negative thermal expansion in framework compound AgB $(CN)_4$ via the concept of average atomic volume. *J. Am. Chem. Soc.* **2020**, *142*, 6935−6939.
(26) Gao, Q. L.; Shi, N. K.; Sanson, A.; Sun, Y.; Milazzo, R.; Olivi, L.; Zhu, H.; Lapidus, S. H.; Zheng, L. R.; Chen, J.; Xing, X. R. Tunable Thermal Expansion from Negative, Zero, to Positive in Cubic Prussian Blue Analogues of $GaFe(CN)_6$. *Inorg. Chem.* **2018**, *57*, 14027−14030.
(27) Schneider, C.; Bodesheim, D.; Ehrenreich, M. G.; Crocellà, V.; Mink, J. n.; Fischer, R. A.; Butler, K. T.; Kieslich, G. Tuning the Negative Thermal Expansion Behavior of the Metal−Organic Framework Cu_3BTC_2 by Retrofitting. *J. Am. Chem. Soc.* **2019**, *141*, 10504−10509.
(28) Yang, C.; Zhang, Y. G.; Bai, J. M.; Qu, B. Y.; et al. Crossover of thermal expansion from positive to negative by removing the excess fluorines in cubic ReO_3-type $TiZrF_{7-x}$. *J. Mater. Chem. C* **2018**, *6*, 5148−5152.
(29) Greve, B. K.; Martin, K. L.; Lee, P. L.; Chupas, P. J.; Chapman, K. W.; Wilkinson, A. P. Pronounced Negative Thermal Expansion from a Simple Structure: Cubic ScF_3. *J. Am. Chem. Soc.* **2010**, *132*, 15496−15498.
(30) Hancock, J. C.; Chapman, K. W.; Halder, G. J.; Morelock, C. R.; Kaplan, B. S.; Gallington, L. C.; Bongiorno, A.; Han, C.; Zhou, S.; Wilkinson, A. P. Large Negative Thermal Expansion and Anomalous Behavior on Compression in Cubic ReO_3-Type A(II)B(IV)F(6): $CaZrF_6$ and $CaHfF_6$. *Chem. Mater.* **2015**, *27*, 3912−3918.
(31) Tallentire, S. E.; Child, F.; Fall, I.; Vella-Zarb, L.; Evans, I. R.; Tucker, M. G.; Keen, D. A.; Wilson, C.; Evans, J. S. Systematic and Controllable Negative, Zero, and Positive Thermal Expansion in Cubic Zr_{1-x} Sn_x Mo_2O_8. *J. Am. Chem. Soc.* **2013**, *135*, 12849−12856.
(32) Hu, L.; Qin, F. Y.; Sanson, A.; Huang, L. F.; Pan, Z.; Li, Q.; Sun, Q.; Wang, L.; Guo, F. M.; Aydemir, U.; Ren, Y.; Sun, C. J.; Deng, J. X.; Aquilanti, G.; Rondinelli, J. M.; Chen, J.; Xing, X. R. Localized Symmetry Breaking for Tuning Thermal Expansion in ScF_3 Nanoscale Frameworks. *J. Am. Chem. Soc.* **2018**, *140*, 4477−4480.
(33) Chen, J.; Gao, Q. L.; Sanson, A.; Jiang, X. X.; Huang, Q. Z.; Carnera, A.; Rodriguez, C. G.; Olivi, L.; Wang, L.; Hu, L.; Lin, K.; Ren, Y.; Lin, Z. S.; Wang, C.; Gu, L.; Deng, J. X.; Attfield, J. P.; Xing, X. R. Tunable thermal expansion in framework materials through redox intercalation. *Nat. Commun.* **2017**, *8*, 14441.
(34) Qin, F.; Chen, J.; Aydemir, U.; Sanson, A.; et al. Isotropic Zero Thermal Expansion and Local Vibrational Dynamics in (Sc, Fe) F_3. *Inorg. Chem.* **2017**, *56*, 10840−10843.
(35) Kennedy, B. J.; Vogt, T. Powder X-ray diffraction study of the rhombohedral to cubic phase transition in TiF_3. *Mater. Res. Bull.* **2002**, *37*, 77−83.
(36) Hu, L.; Chen, J.; Sanson, A.; Wu, H.; Guglieri Rodriguez, C. G.; Olivi, L.; Ren, Y.; Fan, L. L.; Deng, J. X.; Xing, X. R. New Insights into the Negative Thermal Expansion: Direct Experimental Evidence for the "Guitar-String" Effect in Cubic ScF_3. *J. Am. Chem. Soc.* **2016**, *138*, 8320−8323.
(37) Liu, G.; Gao, Z. B.; Ren, J. Anisotropic thermal expansion and thermodynamic properties of monolayer beta-Te. *Phys. Rev. B* **2019**, *99*, 195436.
(38) Li, C. W.; Tang, X. L.; Muñoz, J. A.; Keith, J. B.; Tracy, S. J.; Abernathy, D. L.; Fultz, B. Structural Relationship between Negative Thermal Expansion and Quartic Anharmonicity of Cubic ScF_3. *Phys. Rev. Lett.* **2011**, *107*, 195504.
(39) Wei, Z. S.; Tan, L.; Cai, G. Q.; Phillips, A. E.; da Silva, I.; Kibble, M. G.; Dove, M. T. Colossal Pressure-Induced Softening in Scandium Fluoride. *Phys. Rev. Lett.* **2020**, *124*, 255502.
(40) Zhou, J. J.; Park, J.; Timrov, I.; Floris, A.; Cococcioni, M.; Marzari, N.; Bernardi, M. Ab Initio Electron-Phonon Interactions in Correlated Electron Systems. *Phys. Rev. Lett.* **2021**, *127*, 126404.
(41) Han, F.; Chen, J.; Hu, L.; Ren, Y.; Rong, Y. C.; Pan, Z.; Deng, J. X.; Xing, X. R. The Distortion-Adjusted Change of Thermal Expansion Behavior of Cubic Magnetic Semiconductor $(Sc_{1-x}M_x)F_3$ (M = Al, Fe). *J. Am. Chem. Soc.* **2016**, *99*, 2886−2888.
(42) Perebeinos, V.; Vogt, T. Jahn-Teller transition in TiF_3 investigated using density-functional theory. *Phys. Rev. B: Condens. Matter Mater. Phys.* **2004**, *69*, 115102.

https://doi.org/10.1021/acs.inorgchem.2c03499
Inorg. Chem. 2022, 61, 21004−21010

(43) Hu, L.; Chen, J.; Fan, L.; Ren, Y.; Huang, Q.; Sanson, S.; Jiang, Zh.; Zhou, M.; Rong, Y.; Wang, Y.; Deng, J.; Xing, X. High-Curie-Temperature Ferromagnetism in (Sc,Fe)F_3 Fluorides and its Dependence on Chemical Valence. *Adv. Mater.* **2015**, *27*, 4592−4596.
(44) Cao, Y.; Ji, W.; Lin, K.; Lin, H.; Li, Q.; Wang, C. W.; Wang, N.; Deng, J.; Chen, J.; Xing, X. Zero Thermal Expansion and Strong Covalent Binding of VB_2 Compound. *Inorg. Chem.* **2021**, *60*, 10095−10099.
(45) Lin, K.; Li, Q.; Yu, R.; Chen, J.; Attfield, J. P.; Xing, X. Chemical pressure in functional materials. *Chem. Soc. Rev.* **2022**, *51*, 5351−5364.
(46) Ma, J.; Yang, R.; Chen, H. A large modulation of electron-phonon coupling and an emergent superconducting dome in doped strong ferroelectrics. *Nat. Commun.* **2021**, *12*, 2314.
(47) Wendt, D.; Bozin, E.; Neuefeind, J.; Page, K.; Ku, W.; Wang, L.; Fultz, B.; Tkachenko, A. V.; Zaliznyak, I. A. Entropic elasticity and negative thermal expansion in a simple cubic crystal. *Sci. Adv.* **2019**, *5*, No. eaay2748.

https://doi.org/10.1021/acs.inorgchem.2c03499
Inorg. Chem. 2022, 61, 21004−21010